Available online at www.sciencedirect.com
SCIENCE DIRECT®
Journal of Power Sources 124 (2003) 26–33
JOURNAL OF POWER SOURCES
www.elsevier.com/locate/jpowsour

Sinterability and ionic conductivity of coprecipitated $Ce_{0.8}Gd_{0.2}O_{2-\delta}$ powders treated via a high-energy ball-milling process

T.S. Zhang [a,*], J. Ma [a], L.B. Kong [a], P. Hing [a], Y.J. Leng [b], S.H. Chan [b], J.A. Kilner [c]

[a] *School of Materials Engineering, Nanyang Technological University, Nanyang Avenue, Singapore 639798, Singapore*
[b] *School of Mechanical and Production Engineering, Nanyang Technological University, Nanyang Avenue, Singapore 639798, Singapore*
[c] *Department of Materials, Imperial College of Science, Technology and Medicine, London SW7 2AZ, UK*

Received 19 March 2003; accepted 19 May 2003

Abstract

Ceria-based solid solutions are promising electrolytes for intermediate-temperature, solid oxide fuel cells. The effect of a dry, high-energy, ball-milling process on the sintering and densification behaviour of coprecipitated ceria-based powders is investigated by means of X-ray diffraction, Brunauer–Emmett–Teller (BET) surface-area measurements, density measurements, and electron microscopy. The dry ball-milling process leads to (i) a larger specific surface-area with weak agglomeration; (ii) rearrangement of grains into dense granules; (iii) a higher green density. These effects significantly reduce sintering temperatures and promote densification of ceria-based ceramics. Moreover, a comparison is made of the sintering behaviour and ionic conductivity of the milled samples with and without cobalt oxide doping. Cobalt oxide is a very effective sintering aid, but usually results in an enlarged grain-boundary effect for Si-containing samples. Thus, since SiO_2 is a ubiquitous background impurity in both raw materials and ceramic processing, the dry ball-milling process is a more feasible method for improving the sinterability of coprecipitated ceria-based powders.

Keywords: Ceramic; Sintering; Ceria; Electrolyte; Solid oxide fuel cell; Ball-milling

1. Introduction

Recently, an intensive investigation has been conducted to reduce the operating temperature of solid oxide fuel cells (SOFCs) down to 800–500 °C. Ceria-based solid solutions, such as 20 at.% (atomic ratio) Gd- or Sm-doped ceria, have been regarded as the most promising electrolytes for Intermediate Temperature SOFCs (IT-SOFCs) because they have much higher ionic conductivity than ytrria-stabilised zirconia (YSZ) [1,2]. Being a refractory material, however, CeO_2-based materials are difficult to densify, even when sintered at higher temperature for a long time [3,4]. Such treatment leads to a high manufacturing cost for SOFC systems because ceria-based electrolyte and other components such as the cathode and the anode cannot be co-fired at high temperatures (e.g. >1300 °C).

In order to reduce sintering temperatures, various aqueous-solution-based precipitation systems have been exploited for preparing nanocrystalline ceria-based powders. These include precipitation using ammonia [5], ammonium carbonate [6], hydrazine hydrate [7], oxalic acid precipitant [8,9], forced hydrolysis of inorganic salts [10], urea-based homogeneous precipitation [11], and hexamethylenetetramine (HMT)-based homogeneous precipitation [12]. Among these precipitation systems, oxalate precipitation and HMT-based homogeneous precipitation are most useful for obtaining better ceria-based powders.

Even though these co-precipitated powders are used as precursors, a higher sintering temperature (∼1300–1400 °C) is still needed to obtain dense ceramics [5,6,9,11]. Recently, some transition metal oxides (TMOs), such as cobalt oxide and manganese oxide, have been exploited as sintering aids for ceria-based solid solutions [13,14]. Although these sintering aids can reduce sintering temperatures, they usually cause a remarkable deterioration in the grain-boundary conduction of ceria-based solid solutions, especially for Si-containing samples [15,16]. Considering that SiO_2 is a ubiquitous background impurity in ceramic processing, it is difficult to avoid its presence even when using a relatively pure sample. This study demonstrates that the sintering temperature of a co-precipitated ceria-based powder can be reduced remarkably by treating these powders via a dry

* Corresponding author.
E-mail address: tszhang@ntu.edu.sg (T.S. Zhang).

0378-7753/$ – see front matter © 2003 Published by Elsevier B.V.
doi:10.1016/S0378-7753(03)00625-6

ball-milling process. The effect of cobalt oxide doping on densification, microstructure and electrical properties is also discussed and presented.

2. Experimental procedure

2.1. Preparation of raw powders

An oxalate co-precipitation method was used to prepare the precursor powder of $Ce_{0.8}Gd_{0.2}O_{2-\delta}$ ceramics. High purity (>99.5%) reagents $Ce(NO_3)_3{\cdot}6H_2O$ and $Gd(NO_3)_3{\cdot}6H_2O$ were used as starting materials. Oxalic acid solution was employed as a co-precipitation medium. The preparation procedure is as follows. $Ce(NO_3)_3{\cdot}6H_2O$ and $Gd(NO_3)_3{\cdot}6H_2O$ were dissolved in distilled water, respectively. A mixture of Gd^{3+} and Ce^{3+} ions was prepared by blending the two solutions. The mixture was added to the oxalic acid solution at ~60 °C. During this process, the precipitant solution was controlled at pH = 6.5–7 by dropwise addition of diluted ammonia, and was stirred constantly. After the co-precipitation was completed, the co-precipitate was stirred at ~60 °C for 1 h. The co-precipitate was washed several times using distilled water, then redispersed and washed twice in ethanol, and finally dried at ~100 °C for 20 h. A dry ball-milling process was carried out for 5 h on the co-precipitated powder calcined at 600 °C for 2 h using a high-energy planetary mill, which has been described elsewhere [17].

2.2. Characterisation of samples

Thermal gravimetric–differential thermal analysis (TG–DTA) was conducted on the co-precipitated powder with a heating rate of 5 °C min^{-1} up to 1000 °C in air. The crystal phase was analysed using X-ray diffraction (XRD) with Cu Kα radiation. The particle-size distribution was measured using a laser particle-size analyser. Specific surface-area was estimated by the Brunauer–Emmett–Teller (BET) method with nitrogen as the absorption gas. The morphology of particles was observed by means of scanning electron microscopy (SEM).

The milled and unmilled powders were compacted at 100 MPa into pellets using a stainless-steel die (10 mm diameter) and sintered at temperatures between 900 and 1400 °C for 3 h. The densities of green and sintered pellets were calculated from the mass and dimension of the samples, and measured using the Archimedes method with water. The microstructure of the sintered samples (i.e. well-polished surface after thermal etching) was observed using SEM, and the grain size was calculated from the micrographs using the linear intercept technique. The ionic conductivities of the samples were measured from 250 to 650 °C in air by two-probe impedance spectroscopy (Solartron 1260, UK). A software package was also used to separate the grain-interior (GI) and the grain-boundary (GB) contributions to the total conductivity. In this study, five types of samples were selected to study the effect of SiO_2 or/and Co-oxide doping on ionic conductivity (Table 1).

3. Results and discussion

3.1. Powder characteristics and compact behaviour

The TG–DTA results of the co-precipitate powder are shown in Fig. 1. As in the study of Higashi et al. [9]

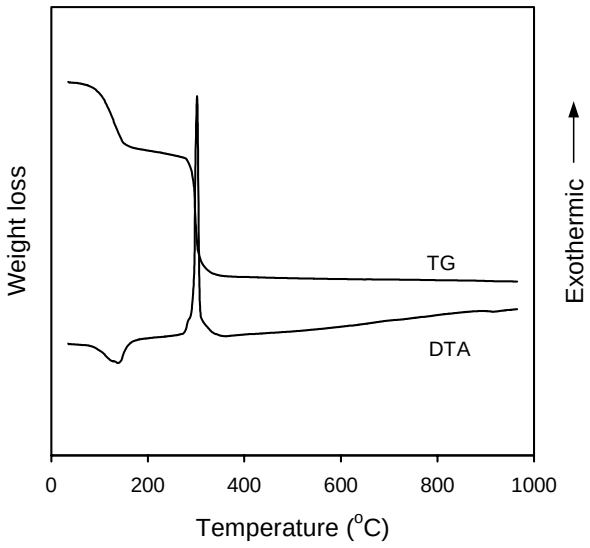

Fig. 1. TG–DTA curves of co-precipitated powder conducted at a heating rate of 5 °C min^{-1} to 1000 °C in air.

Table 1
Characteristics of samples selected for measurement of electrical properties

Sample	Composition	Sintering temperature (°C)/time (h)	Relative density (%)	Grain size (μm)
1	$Ce_{0.8}Gd_{0.2}O_{1.9}$	1150/3	98.5	0.5
2	$Ce_{0.8}Gd_{0.2}O_{1.9}$ + 1 at.% Co-oxide	1100/3	99.3	1.2
3	$Ce_{0.8}Gd_{0.2}O_{1.9}$ + 0.2 at.% SiO_2	1150/3	98.6	0.5
4	$Ce_{0.8}Gd_{0.2}O_{1.9}$ + 0.2 at.% SiO_2 + 1 at.% Co-oxide	1100/3	99.5	1.2
5	$Ce_{0.8}Gd_{0.2}O_{1.9}$ + 0.2 at.% SiO_2 + 1 at.% Co-oxide	1400/3	99.4	–

Milled powder used as precursor powder. SiO_2 or/and Co-oxide loaded into $Ce_{0.8}Gd_{0.2}O_{1.9}$ ceramics via wet chemical method using tetraethoxysilane and cobalt nitrate as starting chemicals.

Table 2
Characteristics of milled and unmilled $Ce_{0.8}Gd_{0.2}O_{1.9}$ powders

	BET surface-area (S_B) ($m^2\ g^{-1}$)	Grain size (R_B) (nm)	Crystallite size (R_X) (nm)
Unmilled powder	37.2	22.52	18.52
Milled powder	45.3	18.42	17.7

at ∼175 °C, the co-precipitated powder loses chemically-adsorbed water and decomposes to oxides at ∼325 °C; no remarkable changes can be detected above 350 °C in both the TG and DTA curves. The sample calcined at 400 °C shows a very broad XRD peak at 2θ =∼29°, which indicates that this sample has low crystallinity. When the calcination temperature is around 600 °C or above, however, the crystalline phase is well-developed. Some powder characteristics of the sample calcined at 600 °C before and after high-energy ball-milling are summarised in Table 2. The mean crystallite size (R_x) was determined by means of the X-ray line broadening method. The mean particle size (R_B) was calculated from BET surface-area data.

Both the particle size and particle-size distribution of the sample calcined at 600 °C were changed during the high-energy ball-milling process. This was measured by a laser particle-size analyser; the results are shown in Fig. 2. The sample before milling has a bimodal particle-size distribution. After milling, the sample shows a very narrow, log-normal, particle-size distribution, although the mean particle size is bigger than that in the unmilled sample. Electron micrographs (Fig. 3) also reveal that there is a large change in particle morphology and size in milled and unmilled samples. The unmilled sample consists of loose agglomerates, as shown in Fig. 3(a). This is the typical microstructure of co-precipitated powders. By contrast, the milled sample (Fig. 3(b)) is composed of granules with nearly spherical shape of size ∼0.5–5 μm.

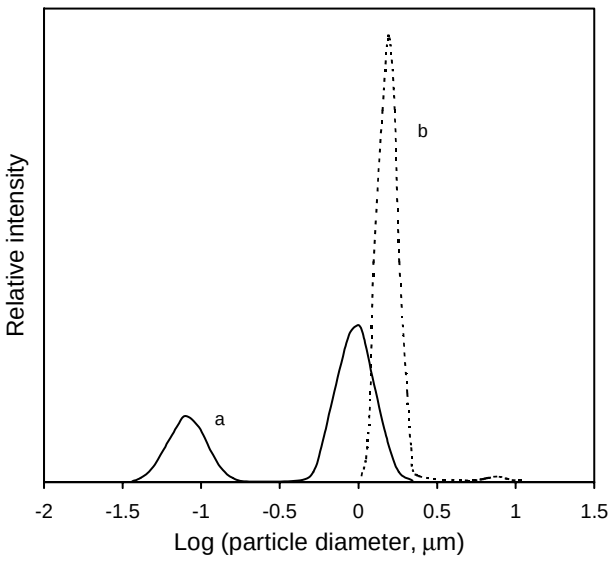

Fig. 2. Particle-size distribution of (a) unmilled and (b) milled powders.

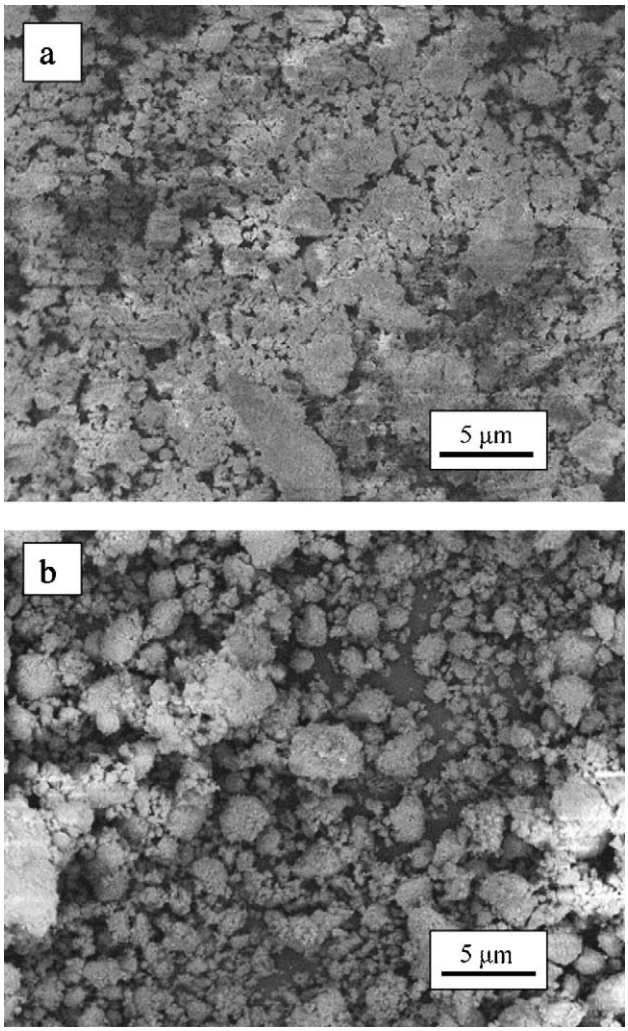

Fig. 3. Electron micrographs of (a) unmilled and (b) milled powders.

The effect of compaction pressure on the green density for the powder calcined at 600 °C, with and without dry-milling, is shown in Fig. 4. A curve with two well-defined linear parts that intersect at a pressure, P_j, is obtained for the unmilled powder. The value of P_j is a measure of agglomerate compression strength, which is to a large extent related to the strength of agglomerates in powders. This strength strongly depends on the preparation method and washing media. Hard agglomerates are particularly detrimental to compaction and sintering behaviour. In this study, the co-precipitated precursor of Gd-doped CeO_2 was redispersed and washed twice in ethanol. This is an important step for obtaining a better precursor powder. Otherwise, the Gd-doped CeO_2 powder shows a very poor sinterability, even though the powder is treated by the dry ball-milling process. Another important point is that the dry ball-milling process is a more effective method only for the ethanol-washed precipitated powders calcined below 800 °C. This may be due to the fact that a higher calcination temperature makes agglomerates so strong that they cannot be broken down via the ball-milling process.

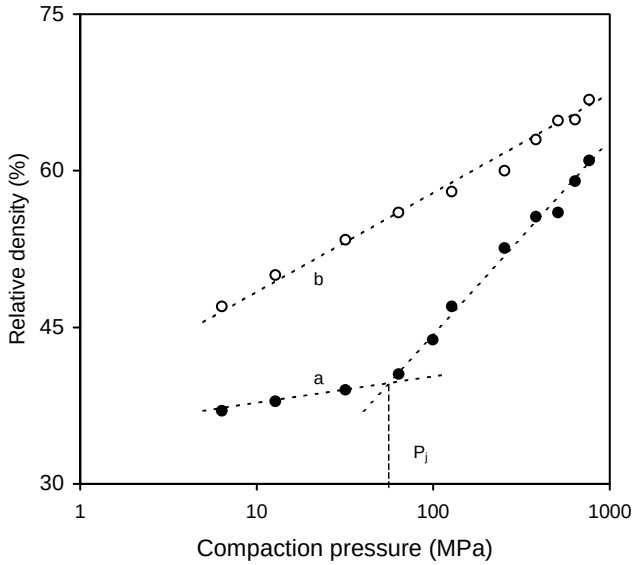

Fig. 4. Compaction behaviour of (a) unmilled and (b) milled powders.

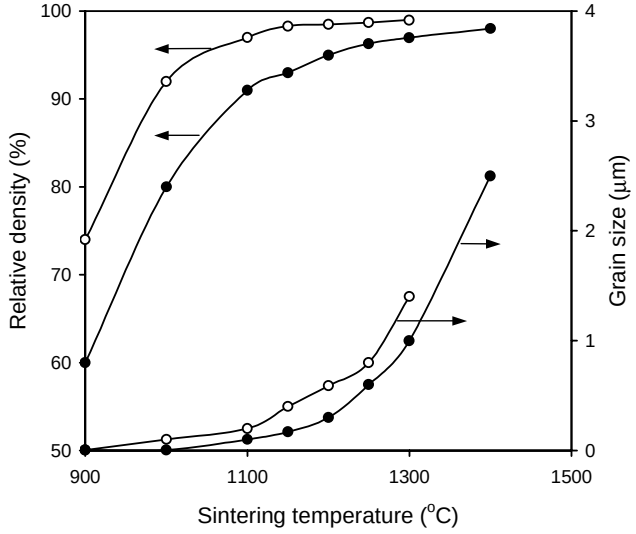

Fig. 5. Effect of sintering temperature for 3 h on density and grain size of (●) unmilled and (○) milled samples.

The value of P_j in this work is around 55 MPa, which is much lower than values reported for zirconia-based powders prepared by different methods [18,19]. Nevertheless, it is higher than the range of 5–40 MPa reported by Duran et al. [20] and by van de Graaf et al. [21]. The energy produced by dry milling may be sufficiently high to crush these hard agglomerates since no agglomerate compression strength (P_j) is found in the curve of green density as a function of log pressure for the milled powders (Fig. 4). This speculation is further confirmed by studying the values of BET surface-area and crystallite size in Table 2 for the milled and unmilled samples. Since both samples show almost the same crystallite size, the larger BET surface-area for the milled sample can only result from the fragmentation of hard agglomerates. Moreover, during the dry-milling process, the particles are rearranged to form the kind of granules shown in Fig. 3(b). Compared with the loose agglomerates in the unmilled powder (Fig. 3(a)), these granules are denser, but they are easy to deform under pressure since the strength of agglomerates is weak in the milled sample. This is why at the same pressure the green density of the milled sample is much higher than the unmilled sample, as shown in Fig. 4.

3.2. Sintering behaviour and microstructure

The sintered densities and grain size of the milled and unmilled samples are given in Fig. 5. At all the temperatures used, the milled sample is denser than the unmilled counterpart. The better sinterability of the milled sample could be a consequence of several factors: (i) the larger specific surface-area with weak agglomeration (Table 2); (ii) the rearrangement of grains into dense granules (Fig. 3(b)); (iii) a higher green density (at 100 MPa, ~58% relative density for the milled sample but only ~45% relative density for the unmilled sample).

At 1150 °C, over 98% relative density can be reached in 3 h for the milled sample. This sample has a very uniform morphology and grain size (~0.5 μm), see Fig. 6. Under the same conditions, however, the unmilled sample has only 93% relative density. Many large interagglomerate pores are not removed, as shown in Fig. 6(b), although this sample has a smaller mean grain size (~0.2 μm). To obtain >98% relative density without milling, a sintering temperature greater than 1400 °C is usually needed to remove the large pores. On the other hand, such a high temperature causes rapid grain growth, for example, grains >2.5 μm in diameter are observed in the unmilled sample sintered at 1400 °C for 3 h. Further reduction in sintering temperature can be achieved for the milled powder by small additions of cobalt oxide. As shown in Fig. 6(c), a nearly full-dense, Gd-doped, CeO_2 ceramic (>99.0% relative density) with the addition of 1 at.% cobalt oxide can be obtained at 1050 °C for 3 h. This sample has a mean grain size of ~100 nm. This result agrees well with that reported by Keinlogel and Gauckler [14]. It is confirmed that for some TMOs (e.g. cobalt oxide) doping leads to the occurrence of viscous flow sintering during the early-stage sintering of ceria-based materials [22]. A significant rearrangement of particles in a compact during early-stage sintering makes the sample denser, and increases the contact area between the particles. This promotes further densification during final-stage sintering. It should be pointed out, however, that a significant reduction in sintering temperatures by addition of cobalt oxide can be observed only for the milled powder.

3.3. Electrical properties

The ionic conductivity of $Ce_{0.8}Gd_{0.2}O_{2-\delta}$-based ceramics was measured by two-probe complex impedance spectroscopy. The interpretation of impedance data for

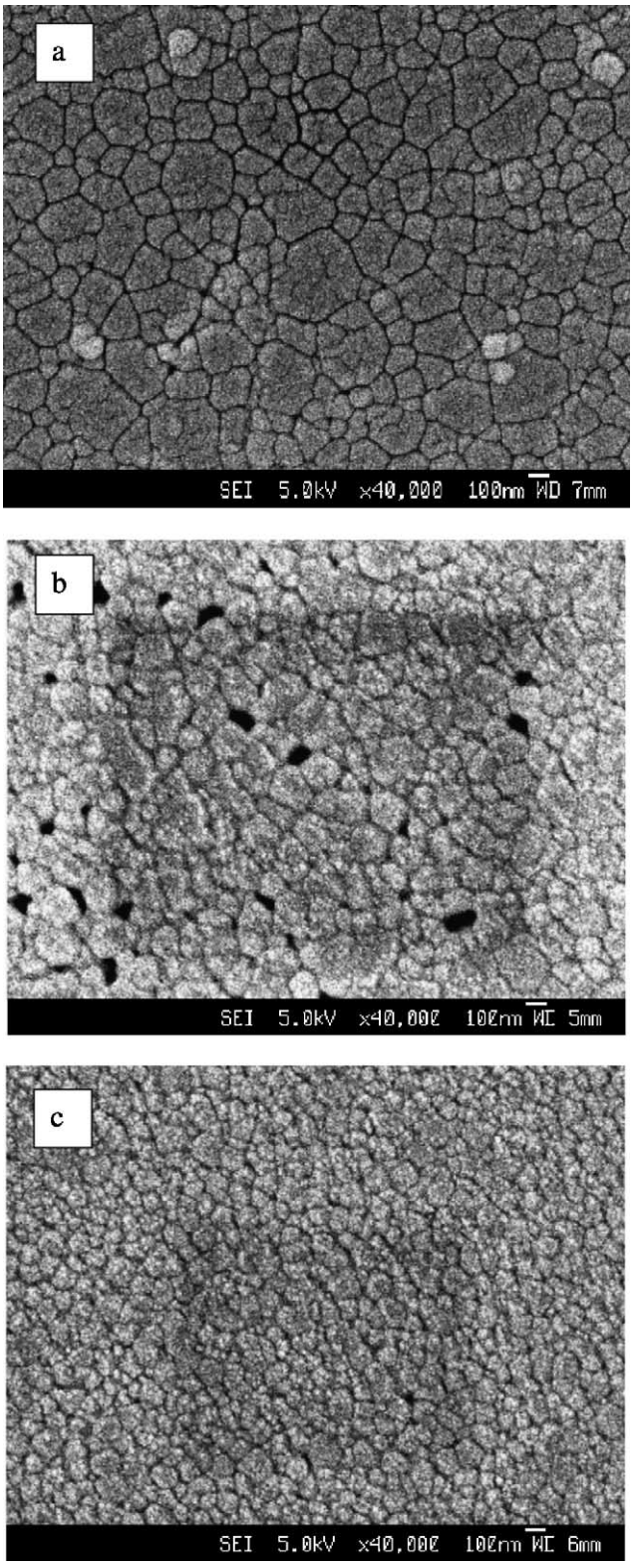

Fig. 6. Electron micrographs of (a) milled and (b) unmilled samples sintered at 1150 °C for 3 h, and (c) milled sample with 1 at.% Co-oxide doping sintered at 1050 °C for 3 h.

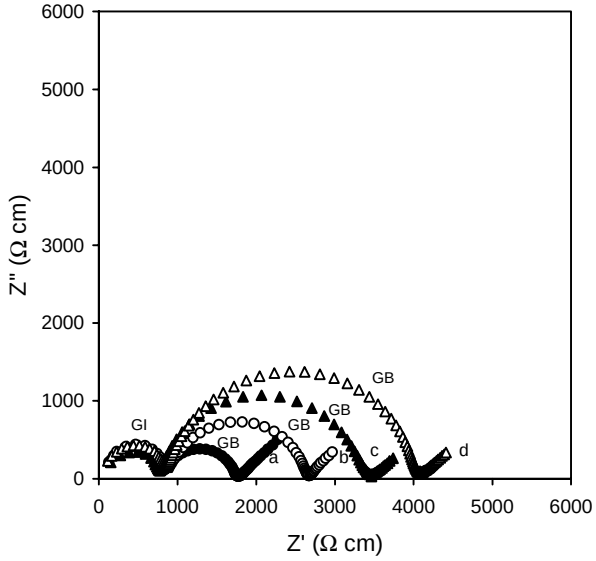

Fig. 7. Impedance spectra measured at 400 °C of (a) undoped $Ce_{0.8}Gd_{0.2}O_{1.9}$, and (b) 0.2 at.% SiO_2, (c) 1 at.% Co-oxide, and (d) 0.2 at.% + 1 at.% Co-oxide-doped $Ce_{0.8}Gd_{0.2}O_{1.9}$ ceramics. GI and GB stand for grain-interior and grain-boundary conductivities, respectively.

polycrystalline materials, such as yttria-stabilised zirconia, has been well documented [23,24]. The impedance spectra of the samples measured at 400 °C in air are given in Fig. 7. It can be seen that the addition of SiO_2 or/and Co-oxide doping enlarges the grain-boundary effect. The quantitative changes in GI and GB conductivities are shown in Figs. 8–10. Inspection of these results indicates that the undoped sample has a smaller grain-boundary effect and a higher total conductivity, and the lower total conductivity for the doped samples results mainly from the enlarged grain-boundary effect since these dopants exert

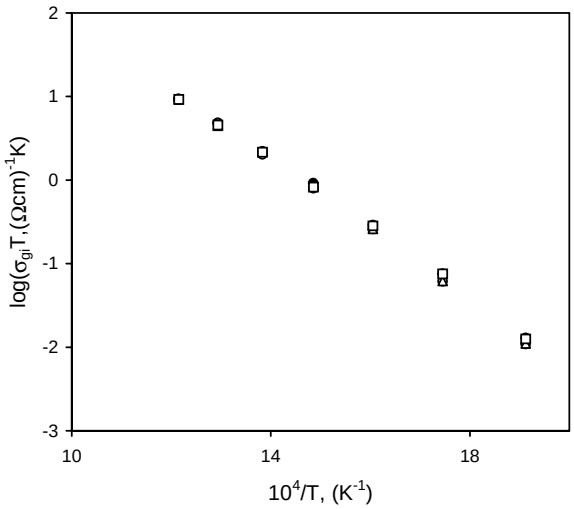

Fig. 8. Arrhenus plot of grain-interior conductivity of (●) undoped $Ce_{0.8}Gd_{0.2}O_{1.9}$, and (○) 0.2 at.% SiO_2, (△) 1 at.% Co-oxide, and (□) 0.2 at.% SiO_2 + 1 at.% Co-oxide-doped $Ce_{0.8}Gd_{0.2}O_{1.9}$ ceramics.

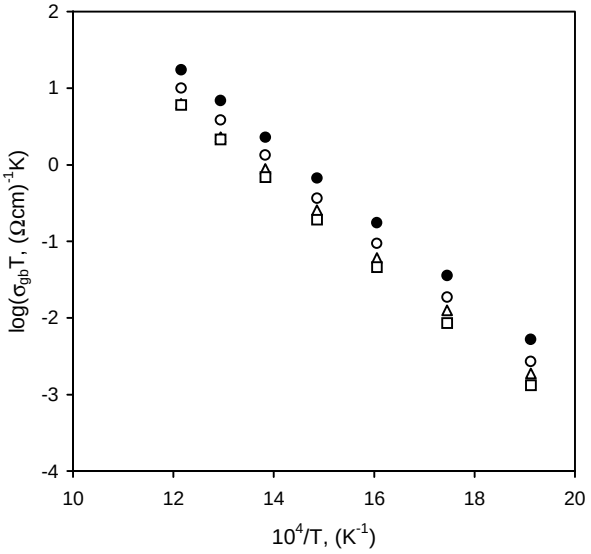

Fig. 9. Arrhenus plot of grain-boundary conductivity of (●) undoped $Ce_{0.8}Gd_{0.2}O_{1.9}$, (○) 0.2 at.% SiO_2, (△) 1 at.% Co-oxide, and (□) 0.2 at.% SiO_2 + 1 at.% Co-oxide-doped $Ce_{0.8}Gd_{0.2}O_{1.9}$ ceramics.

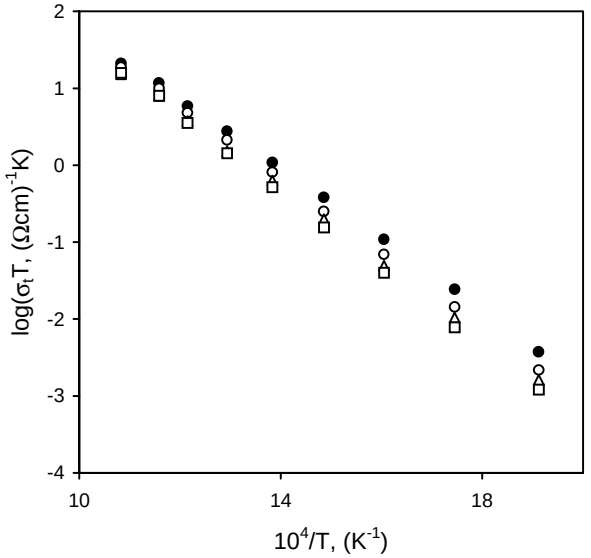

Fig. 10. Arrhenus plot of total conductivity of (●) undoped $Ce_{0.8}Gd_{0.2}O_{1.9}$, (○) 0.2 at.% SiO_2, (△) 1 at.% Co-oxide, and (□) 0.2 at.% SiO_2 + 1 at.% Co-oxide-doped $Ce_{0.8}Gd_{0.2}O_{1.9}$ ceramics.

little influence on the GI conductivity, as shown in Fig. 8. The ionic conductivities and activation energies for conduction in undoped and doped $Ce_{0.8}Gd_{0.2}O_{1.9}$ ceramics are summarised in Table 3.

It is widely accepted that a SiO_2-rich GB phase leads to a deterioration in grain-boundary conduction. An amorphous thin SiO_2-rich film is formed between the grains during sintering, and blocks the movement of oxygen ions through the GB, and thus leads to a lower GB conductivity. According to Steele [25], the grain-boundary effect for pure $Ce_{0.9}Gd_{0.1}O_{1.95}$ cannot be detected above 500 °C, but usually dominates the total conductivity up to ~1000 °C for impure $Ce_{0.9}Gd_{0.1}O_{1.95}$ samples. In our case, the exact content of SiO_2 in the samples is unavailable at the present stage. Nevertheless, the results in Figs. 7–10, clearly show that a small amount of SiO_2 doping (0.2 at.%) does enlarge the grain-boundary effect, and that co-doping of SiO_2 and cobalt oxide is extremely detrimental to grain-boundary conduction. The sample with SiO_2 and Co-oxide co-doping also has a higher activation energy for grain-boundary conduction, as listed in Table 3.

It is interesting to note that the Co-oxide doping has little effect on the grain-boundary conduction of the pure $Ce_{0.8}Gd_{0.2}O_{1.9}$ samples (<0.005 at.% (atomic percent) SiO_2) [14,26]. This indicates that the ceria solid solution used in this study is actually impure since cobalt oxide itself does not cause a marked decrease in grain-boundary conductivity. Unlike Mn-oxide doping [15,16], there are almost no literature reports of the effect of Co-oxide doping on the grain-boundary conduction in impure samples. By analogy, however, Co-oxide may have the same effect as Mn-oxide since these two compounds have a very similar chemical nature. Appel and Bonanos [15] found that the co-doping of SiO_2 and MnO_2 led to a pronounced grain-boundary effect in yttria-stabilised zirconia compared with SiO_2 doping alone. Transmission electron microscopy revealed that Mn doping promoted the propagation of SiO_2 along the grain boundaries. Therefore, it is reasonable to deduce that the redistribution of SiO_2 along grain boundaries due to Co-oxide doping leads to an enlarged grain-boundary effect (Fig. 7). Moreover, it should be pointed out that the grain-boundary conduction of impure samples with Co-oxide doping is strongly dependent on the sintering temperature. At 1400 °C, for example, $Ce_{0.8}Gd_{0.2}O_{1.9}$ with 0.2 at.% SiO_2 and 1 at.% Co-oxide

Table 3
Ionic conductivities and activation energies of doped and undoped $Ce_{0.8}Gd_{0.2}O_{1.9}$ ceramics

Composition	$\sigma_{t(500)}$ (Ω^{-1} cm^{-1})[a]	$\sigma_{gi(500)}$ (Ω^{-1} cm^{-1})[a]	$\sigma_{gb(500)}$ (Ω^{-1} cm^{-1})[a]	E_t (eV)	E_{gi} (eV)	E_{gb} (eV)
$Ce_{0.8}Gd_{0.2}O_{1.9}$	5.45×10^{-4}	1.21×10^{-3}	9.87×10^{-4}	0.93	0.83	1.02
$Ce_{0.8}Gd_{0.2}O_{1.9}$ + 1 at.% Co-oxide	2.9×10^{-4}	1.20×10^{-3}	3.81×10^{-4}	0.98	0.84	1.04
$Ce_{0.8}Gd_{0.2}O_{1.9}$ + 0.2 at.% SiO_2	3.74×10^{-4}	1.18×10^{-3}	5.48×10^{-4}	0.97	0.84	1.04
$Ce_{0.8}Gd_{0.2}O_{1.9}$ + 0.2 at.% SiO_2 + 1 at.% Co-oxide	2.31×10^{-4}	1.18×10^{-3}	2.89×10^{-4}	1.02	0.85	1.07

[a] $\sigma_{t(500)}$, $\sigma_{gi(500)}$, and $\sigma_{gb(500)}$ indicate total, grain-interior, and grain-boundary conductivities at 500 °C, respectively.

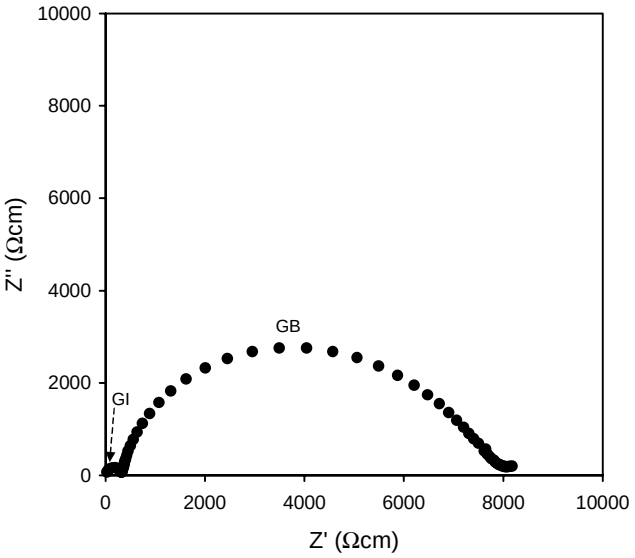

Fig. 11. Impedance spectra measured at 400 °C of 0.2 at.% SiO_2 and 1 at.% Co-oxide co-doped $Ce_{0.8}Gd_{0.2}O_{1.9}$ ceramic sintered at 1400 °C for 3 h, showing a very exaggerated grain-boundary effect compared with the data in Fig. 7.

co-doping shows a very exaggerated GB effect, as shown in Fig. 11.

SiO_2 contamination can result from precursor chemicals since SiO_2 is ubiquitous in raw materials. Moreover, SiO_2 impurity can be introduced from furnace refractories during high-temperature sintering, and can even arise from the silicone grease used in the apparatus to establish input gas mixtures for fuel cell test assemblies [25]. Some Co- or Mn-containing perovskite compounds, such as $La_{0.8}Sr_{0.2}Fe_{0.8}Co_{0.2}O_{3-\delta}$ [27,28] and $La_{0.8}Sr_{0.2}MnO_{3-\delta}$ [29], are widely used as electrodes for SOFCs. During the fabrication and operation of SOFCs, the interaction and interdiffusion of ceria-based electrolytes with electrode materials cannot be easily avoided, and results in the formation of low-conductivity layers at the electrode|electrolyte interface. Therefore, optimisation of the electrode fabrication conditions is essential. On the other hand, the above results also suggest that it is unwise to reduce the sintering temperature and promote densification for ceria-based materials by using these TMOs (e.g. Co-oxide) as sintering aids. Alternatively, the dry ball-milling process is a feasible method for improving the sinterability of co-precipitated ceria-based electrolytes.

4. Conclusions

The dry, high-energy, ball-milling process remarkably changes the particle morphology, the strength and extent of agglomeration, and the compaction behaviour of co-precipitated powder calcined at 600 °C in 3 h. The washing media and calcining temperature are important factors that affect the sinterability of the milled powder. For ethanol-washed precipitated powder calcined at 600 °C for 3 h, after 6 h of dry ball-milling, over 98% relative density can be obtained at 1150 °C in 3 h compared with only ∼93% relative density for the unmilled sample.

Further reduction in sintering temperature can be achieved for the milled powder by small additions of cobalt oxide. The addition of 1 at.% Co-oxide leads to a nearly fully-dense ceria ceramic (>99.0% relative density) at 1050 °C in 3 h with a grain size of ∼100 nm. It is found, however, that Co-oxide doping has a detrimental effect on GB behaviour for Si-containing samples, and this leads to a lower total conductivity. As SiO_2 is a ubiquitous background impurity, it is therefore unsuitable to use Co-oxide as a sintering aid for the densification of ceria-based electrolytes. This also suggests that optimisation of the electrode fabrication conditions is necessary, since many Co-containing perovskite compounds are widely used as electrodes for SOFCs.

References

[1] L. Navarro, F. Marques, J. Frade, J. Electrochem. Soc. 144 (1997) 267.
[2] M. Godickemeier, K. Sasaki, L.J. Gauckler, J. Electrochem. Soc. 144 (1997) 1635.
[3] K. El Adham, A. Hammou, J. Chim. Phys. Phys. Chim. Biol. 79 (1982) 633.
[4] H. Yahiro, Y. Baba, K. Eguchi, H. Arai, J. Electrochem. Soc. 135 (1988) 2077.
[5] Y.M. Chiang, E.B. Lavik, D.A. Blom, Nanostruct. Mater. 9 (1997) 633.
[6] Y.M. Chiang, E.B. Lavik, I.K. Osack, H.L. Tuller, J.M. Ying, J. Electroceram. 1 (1997) 7.
[7] T.J. Kirk, J. Winnick, J. Electrochem. Soc. 140 (1993) 3494.
[8] J. Varele, T. Horita, T. Kawada, N. Sakai, H. Yokokawa, M. Dokiya, J. Eur. Ceram. Soc. 16 (1996) 961.
[9] K. Higashi, K. Sonada, H. Ono, S. Sameshima, J. Mater. Res. 14 (1999) 957.
[10] V. Briois, C.E. Williams, H. Dexpert, F. Villain, B. Cabane, F. Deneuve, C. Magnier, J. Mater. Sci. 28 (1993) 5019.
[11] X. Chu, W. Chung, L.D. Schmidt, J. Am. Ceram. Soc. 76 (1993) 2115.
[12] P.L. Chen, I.W. Chen, J. Am. Ceram. Soc. 76 (1993) 1577.
[13] C. Keinlogel, L.J. Gauckler, Solid State Ionics 135 (2000) 567.
[14] C. Keinlogel, L.J. Gauckler, Adv. Mater. 13 (2001) 1081.
[15] C.C. Appel, N. Bonanos, J. Eur. Ceram. Soc. 19 (1999) 847.
[16] T.S. Zhang, L.B. Kong, Z.Q. Zeng, H. Huang, P. Hing, J. Kilner, J. Solid State Electrochem. 7 (2003) 348.
[17] L.B. Kong, J. Ma, T.S. Zhang, W. Zhu, O.K. Tan, J. Mater. Sci. Mater. Electron. 13 (2000) 89.
[18] M.A.C.G. van der Graaf, A.J. Burggraaf, Advances in Ceramics, Science and Technology of Zirconia II, vol. 12, p. 744.
[19] J.L. Shi, Z.X. Lin, W.J. Qian, T.S. Yen, J. Eur. Ceram. Soc. 13 (1994) 265.
[20] P. Duran, M. Villegas, F. Capel, J.F. Fernandez, C. Moure, J. Mater. Sci. 32 (1997) 4507.
[21] M.A.C.G. van de Graaf, J.H. Ter Maat, A.J. Burggraaf, J. Mater. Sci. 20 (1985) 1407.

[22] T.S. Zhang, P. Hing, H. Huang, J. Kilner, J. Mater. Sci. 37 (2002) 997.
[23] J.E. Bauerle, J. Phys. Chem. Solids 30 (1969) 2651.
[24] J.R. Macdonald (Ed.), Impedance Spectroscopy-Emphasizing Solid Materials and Systems, Wiley, New York, 1987.
[25] B.C.H. Steele, Solid State Ionics 129 (2000) 95.
[26] T.S. Zhang, J. Ma, L.B. Kong, P. Hing, J. Kilner, Solid State Ionics, submitted for publication.
[27] S.R. Wang, T. Kato, S. Nagata, T. Honda, T. Kaneko, N. Iwashita, M. Dokiya, Solid State Ionics 146 (2002) 203.
[28] H. Vchida, S. Arisaka, M. Watanabe, Solid State Ionics 135 (2000) 347.
[29] A. Eudo, H. Fukunaga, C. Wen, K. Yamada, Solid State Ionics 135 (2000) 353.